J. Fluid Mech. (2015), *vol.* 771, *pp.* 303–326. © Cambridge University Press 2015
doi:10.1017/jfm.2015.181

Spectral scaling in boundary layers and pipes at very high Reynolds numbers

M. Vallikivi[1], B. Ganapathisubramani[2] and A. J. Smits[1,3,†]

[1]Department of Mechanical and Aerospace Engineering, Princeton University, Princeton, NJ 08544, USA

[2]Aerodynamics and Flight Mechanics Group, Faculty of Engineering and the Environment, University of Southampton, Southampton SO17 1BJ, UK

[3]Department of Mechanical and Aerospace Engineering, Monash University, Melbourne, Australia

(Received 10 June 2014; revised 6 March 2015; accepted 18 March 2015; first published online 21 April 2015)

One-dimensional energy spectra in flat plate zero pressure gradient boundary layers and pipe flows are examined over a wide range of Reynolds numbers ($2600 \leqslant Re_\tau \leqslant 72\,500$). The spectra show excellent collapse with Kolmogorov scaling at high wavenumbers for both flows at all Reynolds numbers. The peaks associated with the large-scale motions (LSMs) and superstructures (SS) in boundary layers behave as they do in pipe flows, with some minor differences. The location of the outer spectral peak, associated with SS or very large-scale motions (VLSMs) in the turbulent wall region, displays only a weak dependence on Reynolds number, and it occurs at the same wall-normal distance where the variances establish a logarithmic behaviour and where the amplitude modulation coefficient has a zero value. The results suggest that with increasing Reynolds number the energy is largely confined to a thin wall layer that continues to diminish in physical extent. The outer-scaled wavelength of the outer spectral peak appears to decrease with increasing Reynolds number. However, there is still significant energy content in wavelengths associated with the SS and VLSMs. The location of the outer spectral peak appears to mark the start of a plateau that is consistent with a k_x^{-1} slope in the spectrum and the logarithmic variation in the variances. This k_x^{-1} region seems to occur when there is sufficient scale separation between the locations of the outer spectral peak and the outer edge of the log region. It does not require full similarity between outer and wall-normal scaling on the wavenumber. The extent of k_x^{-1} region depends on the wavelength of the outer spectral peak (λ_{OSP}), which appears to emerge as a new length scale for the log region. Finally, based on the observations from the spectra together with the statistics presented in Vallikivi *et al.* (*J. Fluid Mech.*, 2015 (submitted)), five distinct wall-normal layers are identified in turbulent wall flows.

Key words: boundary layer structure, pipe flow boundary layer, turbulent boundary layers

1. Introduction

Studies of high-Reynolds-number wall-bounded flows, such as boundary layers and pipes, have shown that at sufficiently high Reynolds numbers these flows have

† Email address for correspondence: asmits@princeton.edu

many characteristics in common (Marusic *et al.* 2010; Smits, McKeon & Marusic 2011; Smits & Marusic 2013). In particular, the mean velocity, the variances and even the higher-order moments of the streamwise velocity fluctuations all demonstrate a logarithmic behaviour in region that, according to Hultmark *et al.* (2012), Hultmark *et al.* (2013), Marusic *et al.* (2013) and Vallikivi, Hultmark & Smits (2015), corresponds to $800 \lesssim y^+ \lesssim 0.15Re_\tau$ in pipes, and $400 \lesssim y^+ \lesssim 0.15Re_\tau$ in boundary layers. Here, $Re_\tau = \delta u_\tau/\nu$ is the friction Reynolds number, ν is the kinematic viscosity, u_τ is the friction velocity, δ is the characteristic shear layer thickness (δ_{99} for boundary layers and the radius R for pipes), y is the wall-normal distance and $y^+ = yu_\tau/\nu$. The upper and lower limits that define this region are still a matter of debate (see, for example, Vincenti *et al.* 2013; Marusic *et al.* 2013), but in what follows we will use the term log-layer to denote the region of the flow where the mean velocity and the variances both follow a logarithmic variation. We also use the term turbulent wall layer to denote the region where $50 \lesssim y^+ \lesssim 0.15Re_\tau$. The origin of the wall-normal dependence in wall-bounded turbulent flows has been linked to the character of the mean governing equation by Fife *et al.* (2005), Fife, Klewicki & Wei (2009), Klewicki, Fife & Wei (2009) and Klewicki (2013*b*), who also identified the asymptotic bounds of the particular domains that exist. As we will see, however, these analyses do not conform to the results obtained at the highest Reynolds numbers considered here.

The distribution of energy among scales is also of great interest. However, experimentally measuring the full three-dimensional energy spectrum is not usually possible, and often we can only examine the power spectral density of the streamwise velocity fluctuations Φ_{uu}, where

$$\overline{u^2} = \int_0^\infty \Phi_{uu}(k_x)\mathrm{d}k_x = \int_0^\infty k_x\Phi_{uu}(k_xy)\mathrm{d}(k_xy). \tag{1.1}$$

Here, $k_x = 2\pi/\lambda_x$ is the streamwise wavenumber, λ_x is the streamwise wavelength and $\overline{u^2}$ is the variance of the streamwise velocity fluctuations. We commonly measure frequency spectra instead of wavenumber spectra, and rely on Taylor's hypothesis (Taylor 1938) to infer λ_x.

Nevertheless, such restricted spectral data can still give valuable insight into the behaviour of wall-bounded turbulence. For instance, in the region where $\nu/u_\tau \ll y \ll \delta$ (typically associated with the log-law in the mean velocity), Perry & Abell (1977) and Perry, Henbest & Chong (1986) suggested that the turbulence spectrum may be divided into three regions: a low-wavenumber range that scales with the characteristic shear layer length scale δ; an intermediate-wavenumber range that scales with the wall-normal distance y; and a high-wavenumber range that scales with the Kolmogorov length scale η_K. Perry & Abell (1977) then argued that at a sufficiently high Reynolds number there may be an overlap of the low- and intermediate-wavenumber regions such that $\Phi_{uu}(k_x) \propto {k_x}^{-1}$, often referred to as the k_x^{-1} law. Similarly, an overlap of the intermediate- and high-wavenumber regions would be expected to occur (for local equilibrium flows), where $\Phi_{uu}(k_x) \propto k_x^{-5/3}$. This is the so-called $k_x^{-5/3}$ law, a result first obtained by Kolmogorov (1941) on dimensional grounds.

The k_x^{-1} dependence is of particular interest here. By integrating over the region where k_x^{-1} holds, from a low-wavenumber limit given by a constant value of $k_x\delta$ to a high-wavenumber limit given by a constant value of k_xy, it follows that the streamwise turbulence intensity will obey, for $y^+ \to \infty$,

$$u^{2+} = B_1 - A_1 \ln\left[\frac{y}{\delta}\right], \tag{1.2}$$

where $u^{2+} = \overline{u^2}/u_\tau^2$, A_1 is a universal constant and B_1 is a large-scale constant (Perry *et al.* 1986). This log-law was first suggested by Townsend (1976) on the basis of the attached eddy hypothesis. Recent measurements by Hultmark *et al.* (2012) in pipes, and Marusic *et al.* (2013) and Vallikivi *et al.* (2015) in boundary layers, have confirmed that this expected logarithmic variation in the variance begins to emerge at sufficiently high Reynolds numbers ($Re_\tau \gtrsim 5000$).

The existence of a k_x^{-1} law plays an important role in turbulence modelling, especially in the framework of Townsend's attached eddy model (Townsend 1976; Perry & Chong 1982; Perry & Li 1990; Marusic, Uddin & Perry 1997; Marusic & Kunkel 2003). Recently, Banerjee & Katul (2013) used a phenomenological explanation for the origin of the log-law for the streamwise turbulent intensity in the intermediate region and showed that this log region would exist if the very large-scale motions (VLSMs) do not disturb the k_x^{-1} scaling in wavenumber spectrum. However, at this time, the k_x^{-1} law has been seen in laboratory flows at high Reynolds number over a very limited spatial extent by Nickels *et al.* (2005) or only in atmospheric boundary layer data (see, for example, Högström, Hunt & Smedman 2002; Katul & Chu 1998; Calaf *et al.* 2013). The k_x^{-1} region is also linked to the notion of complete similarity, in that it is implicitly a region where wall-normal scaling (y and u_τ) and outer scaling (δ and u_τ) occur over the same wavenumber range. Morrison *et al.* (2004) and Rosenberg *et al.* (2013) showed, however, that in pipe flow the spectrum collapsed at low wavenumbers in outer scaling and at intermediate wavenumbers in wall-normal scaling, but there was no overlap region where both scalings held simultaneously (a condition they called incomplete similarity).

The energy distribution in wavenumber space represented by the spectrum can also help to understand the structure of turbulence, especially the behaviour of the coherent motions. Large-scale coherent structures have been observed in boundary layers (Kovasznay, Kibens & Blackwelder 1970; Balakumar & Adrian 2007) and in pipes (Kim & Adrian 1999; Guala, Hommema & Adrian 2006) that are 2–3δ long in the streamwise direction and 1–1.5δ wide in the spanwise direction. These structures are usually referred to as large-scale motions (LSMs), and are associated with the occurrence of bulges of turbulent fluid at the edge of the wall layer. They carry a significant amount of the Reynolds shear stress and play an important role in turbulent transport (Ganapathisubramani, Longmire & Marusic 2003).

Much longer, meandering structures have also been observed. In pipe flows these structures are usually referred to as VLSMs (Kim & Adrian 1999; Guala *et al.* 2006), and they appear to extend up to 20R in the streamwise direction (Monty *et al.* 2007; Bailey & Smits 2010). Similar structures have been observed in boundary layers, extending up to 20δ in length, where they are called superstructures (SS). It is important to note that when inferred from single point statistics, these lengths are usually much shorter, 6δ and 10–15R respectively, due to their meandering nature (Hutchins & Marusic 2007). Hutchins & Marusic (2007) found that the SS scale with the boundary layer thickness δ, and that they are present only in the turbulent wall region, compared with VLSMs that extend throughout the outer flow of pipes and channels. Monty *et al.* (2009) suggested that the differences between VLSM and SS may simply be due to the dissimilar boundary conditions imposed by open and confined geometry flows, and Chung *et al.* (2015) have now proposed a mechanism based on the attached eddy hypothesis that links the flow geometry to the structure of the very large scales.

In the premultiplied spectrum, $k_x\Phi_{uu}$, it is often possible to observe the signature of the coherent motions. In the near-wall region, there is always a single prominent

spectral peak associated with the maximum energy production located around the inner peak in the variance at about $y^+ = 12$–15 (we call this the inner spectral peak). In the outer region, there are often two peaks visible in the premultiplied spectrum, one associated with the VLSMs or SS, and another associated with the LSM (Rosenberg *et al.* 2013), although in boundary layers the LSM peak is usually less distinct than in pipe flows (Hutchins & Marusic 2007). In addition, we can identify the point where the VLSM or SS spectral peak has its maximum magnitude; we shall call this the outer spectral peak, and it is described by a magnitude $(k_x\Phi_{uu})_{OSP}$, a specific physical location y_{OSP}, and a specific wavenumber k_{OSP}. The outer spectral peak corresponds to the point where the spectrum displays the largest energy content per wavenumber outside the viscous wall region.

The location, magnitude and wavelength of these spectral peaks is still an open issue. Hutchins & Marusic (2007) observed the outer spectral peak associated with SS for $Re_\tau \geqslant 2000$ in boundary layers, and found that it was located at about $y/\delta \approx 0.06$ and $\lambda_x/\delta \approx 6$, and that its magnitude increased with Reynolds number. These observations were made on data with $Re_\tau \leqslant 7300$. A considerably larger range, $2800 < Re_\tau < 19\,000$, was available to Mathis, Hutchins & Marusic (2009), and at these Reynolds numbers the footprint of the SS and the presence of the associated outer spectral peak were clearly evident. Mathis *et al.* (2009) calculated Re_τ using $\delta = 1.13\delta_{99}$, so for purposes of comparison it is probably better to state their Reynolds number range as $2500 < Re_\tau < 17\,000$, as noted by Klewicki (2013*a*). Here, we use the range as given by Mathis *et al.* to avoid confusion. They found that the intensity of the large scales in the log-region increased with Reynolds number, increasing the amplitude modulation of the near-wall small-scale structures due to the large scales, and they suggested that the increase in the magnitude of the outer spectral peak, which was attributed to the increasing strength of the VLSMs or SS, was connected to the increase in the near-wall peak in the variance. Mathis *et al.* (2009) found that the outer spectral peak was located at about $y^+ \approx 3.9Re_\tau^{0.5}$ (which they associated with the middle of the log-layer with bounds $100 < y^+ < 0.15Re_\tau$) with a wavelength of $\lambda_x/\delta \approx 3$–$6$ (based on figure 12 of their paper), close to the location where the magnitude of the amplitude modulation correlation was zero. Revisiting these data, however, yields a value for the coefficient of 3 instead of 3.9. This would imply a level of connection to the later finding of Marusic *et al.* (2013) where this point is identified as the beginning of the log region for both the mean flow and the turbulence intensity (for pipes and boundary layers).

There remains the question whether the reported trends persist with increasing Reynolds number, or if some Reynolds-number-independent, self-similar regime might emerge once the scale separation is large enough. To help provide an answer, we present measurements of spectra in boundary layers at Reynolds numbers up to $Re_\tau \approx 70\,000$. At the highest Reynolds number, the mean velocity and variances display a log-layer that extends over more than a decade in wall distance (Vallikivi *et al.* 2015). We also take the opportunity to compare the results with similar measurements in pipe flow by Hultmark *et al.* (2013) and Rosenberg *et al.* (2013) at matching Reynolds numbers.

2. Experiments

The experiments in a zero-pressure-gradient boundary layer were conducted in the High Reynolds number Test Facility (HRTF) for $3300 \leqslant Re_\tau \leqslant 72\,500$. The facility was described by Jiménez, Hultmark & Smits (2010). The behaviour of the mean flow,

Case	Pipe				Boundary layer				
$Re_\tau \approx$	Re_τ	R (mm)	ν/u_τ	ℓ^+	Re_τ	δ_{99} (mm)	ν/u_τ	ℓ^+	Symbol
3×10^3	3 334	64.68	19	3.1	2 622	27.2	10	5.8	▼
5×10^3	5 412	64.68	12	5.0	4 635	27.3	5.9	10	■
10×10^3	10 481	64.68	6.2	9.7	8 261	28.4	3.4	17	▲
20×10^3	20 250	64.68	3.2	18.8	25 062	25.7	1.0	29	◆
40×10^3	37 690	64.68	1.7	35.0	40 053	25.8	0.6	47	◀
70×10^3	68 371	64.68	0.95	31.7	72 526	29.1	0.4	75	●

TABLE 1. Cases chosen for comparing boundary layer and pipe flow behaviour. Pipe flow data from Hultmark *et al.* (2013) and Rosenberg *et al.* (2013). Boundary layer data from Vallikivi *et al.* (2015).

variances, and higher-order moments was reported by Vallikivi *et al.* (2015), where further details of the experiment may be found (see also Vallikivi 2014). Here we choose six Reynolds numbers for detailed comparison of the spectral behaviour with pipe flows (see table 1). Nano-scale thermal anemometry probes (NSTAPs) were used for all measurements (boundary layers and pipes), with a temporal resolution up to 300 kHz and a spatial resolution down to 30 μm (Bailey *et al.* 2010; Vallikivi *et al.* 2011; Vallikivi & Smits 2014).

Taylor's hypothesis (Taylor 1938) was used to convert the frequency spectrum to the spatial spectrum by assuming that the local turbulent field is 'frozen' while it is carried past the sensor at a characteristic convection velocity. We use the local mean velocity as the convection velocity at each wall-normal location. Rosenberg *et al.* (2013) gives an extended discussion on the implications of using Taylor's hypothesis at these Reynolds numbers in pipe flow, and they concluded that, although very close to the wall it can introduce significant distortions, the trends in the spectra (for example, the presence of a k_x^{-1} region) were not significantly affected. We expect that similar considerations will apply to boundary layer flows.

For all cases studied, the sampling frequency $f_s = 300$ kHz, which corresponds to $12.6 < f_s^+ < 0.80$ for the pipe and $9.47 < f_s^+ < 0.45$ for the boundary layer (see table 1, where $f_s^+ = f_s \nu/u_\tau^2$).

To find the Kolmogorov length scale $\eta_K = (\nu^3/\varepsilon)^{1/4}$ and velocity scale $u_K = (\nu\varepsilon)^{1/4}$, the mean dissipation rate ε was found by integrating the one-dimensional dissipation spectrum according to

$$\varepsilon = 15\nu \int_0^\infty k_x^2 \Phi_{uu} \mathrm{d}k_x. \tag{2.1}$$

Bailey *et al.* (2009) measured the local dissipation scales in the pipe facility at lower Reynolds numbers and found the isotropic relation to be a reasonable estimate, similar to six other methods tested. However, for the higher-Reynolds-number cases the dissipation spectra was not fully covered by the measurements, decreasing the accuracy of the ε estimate. This potential source of error is discussed further below.

3. Results and discussion

3.1. *Kolmogorov scaling*

The spectra in Kolmogorov scaling are shown in figure 1 for $0.001 \leqslant y/\delta \leqslant 1.0$ at $Re_\tau \approx 20\,000$. The Kolmogorov scaling collapses the higher wavenumber data well for

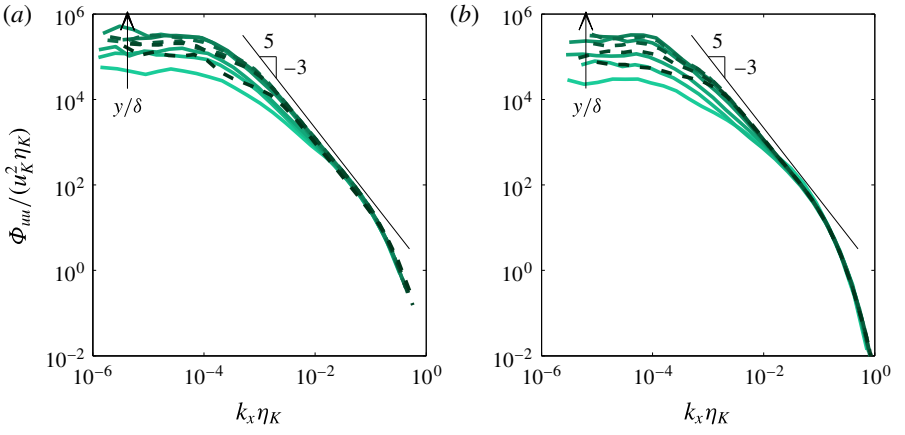

FIGURE 1. (Colour online) Kolmogorov spectra in wall scaling for boundary layer (*a*) and pipe flow (*b*) at wall-normal positions $y/\delta \approx 0.001$, 0.005, 0.01, 0.05, 0.15, 0.3 and 0.5, at $Re_\tau \approx 20\,000$. Solid lines indicate wall locations $y/\delta \leqslant 0.15$, changing to dashed lines for $y/\delta > 0.15$. Arrow indicates increase in y/δ until $y/\delta = 0.15$.

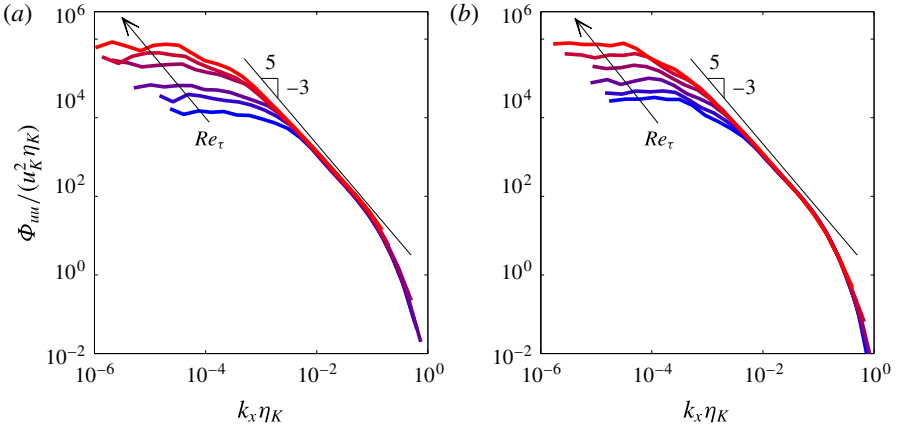

FIGURE 2. (Colour online) Kolmogorov spectra for boundary layer (*a*) and pipe flow (*b*) with $Re_\tau \approx 3\times10^3$, 5×10^3, 10×10^3, 20×10^3, 40×10^3 and 70×10^3, at $y/\delta \approx 0.5$.

both flows at all locations, and as y/δ increases a power law range with a slope close to $-5/3$ emerges, extending a maximum of two decades with an upper limit at $k_x\eta_K \approx 0.1$. The energy at larger length scales (smaller k_x) increases with y/δ, until at $y/\delta > 0.15$ the energy at large scales starts to decrease in the wake region. The extent of the power law region continues to increase with increasing wall distance, but for boundary layers at larger y/δ the spectra depart from this collapse at higher wavenumbers than in pipe flow, which is likely due to the large-scale intermittency in the outer part of the boundary layer.

Figure 2 shows Kolmogorov spectra for all Reynolds numbers at $y/\delta = 0.5$. The behaviour of boundary layer and pipe spectra at higher wavenumber is essentially identical for $Re_\tau \geqslant 5000$, indicating that the smaller wavelengths are largely independent of the flow geometry at these Reynolds numbers. To demonstrate this

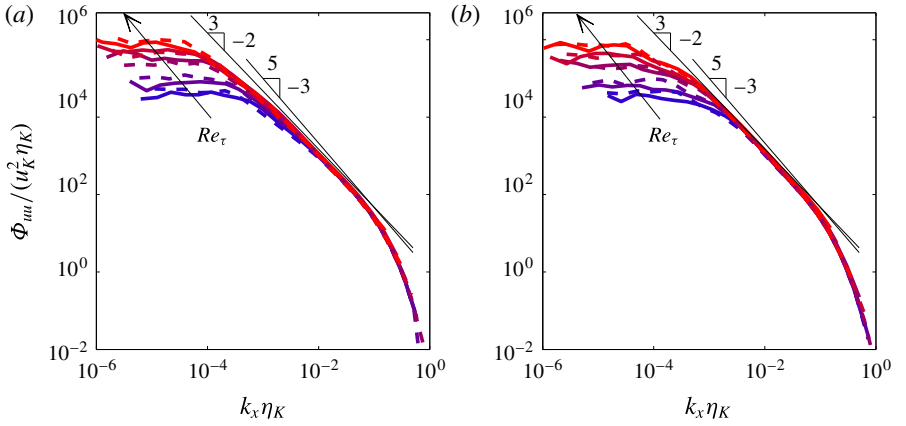

FIGURE 3. (Colour online) Kolmogorov spectra for at $Re_\tau \approx 3 \times 10^3$, 5×10^3, 10×10^3, 20×10^3, 40×10^3, and 70×10^3, at $y/\delta \approx 0.05$ (*a*) and $y/\delta \approx 0.5$ (*b*); ——, boundary layer; – – – –, pipe.

point further, the boundary layer and pipe spectra are plotted together for $y/\delta = 0.05$ and $y/\delta = 0.5$ in Figure 3. We see that the curves collapse very well for the higher wavenumbers, but that they have an exponent that is closer to -1.5 or 1.52 than to $-5/3$. This observation agrees with the work of Mydlarski & Warhaft (1996), Gamard & George (2000), McKeon & Morrison (2007) and George & Tutkun (2009), among others, who propose that viscous effects continue to be important in the inertial region, and that a slope of $-5/3$ is only reached at infinite Reynolds number. For example, Mydlarski & Warhaft (1996) found an empirical relation for the slope given by $(5/3)\ (1\text{–}3.15Re_\lambda^{-2/3})$, where Re_λ is the Reynolds number based on the Taylor microscale. For the current data set, Re_λ varies from about 200 to 1000, where Mydlarski *et al.*'s relationship gives slopes of 1.5–1.6, which agrees well with our observations.

By assuming Kolmogorov scaling to be valid at all Reynolds numbers, the error in finding the mean dissipation ε can be estimated by examining the lack of collapse of the experimental spectra at high wavenumbers. This presumed error was found to increase with Re_τ from 0.5 % to 4 % for the pipe, and from 1 % to 5 % for the boundary layer, with the exception of the boundary layer case at $Re_\tau \approx 70\,000$ where the error in ε was about 20 %. The corresponding maximum error in η_K was therefore always less than 5 %.

3.2. *The* k_x^{-1} *dependence*

To examine the k_x^{-1} dependence, spectra in the usual log–log form are given in figure 4 for $0.001 \leqslant y/\delta \leqslant 0.5$. The spectra are also shown in premultiplied form in figures 5 and 6 at $Re_\tau = 5000$ and 70 000, respectively, and in this form the k_x^{-1} region would show up as a plateau. At both Reynolds numbers, the pipe flow spectra show two peaks: one at lower wavenumbers associated with the VLSM, and another at higher wavenumbers associated with the LSM (Balakumar & Adrian 2007). For boundary layers, the lower wavenumber peak associated with the SS (Hutchins & Marusic 2007) is present at all Reynolds numbers, while the higher-wavenumber LSM peak only appears at some Reynolds numbers at some locations. This is illustrated more precisely in figure 7.

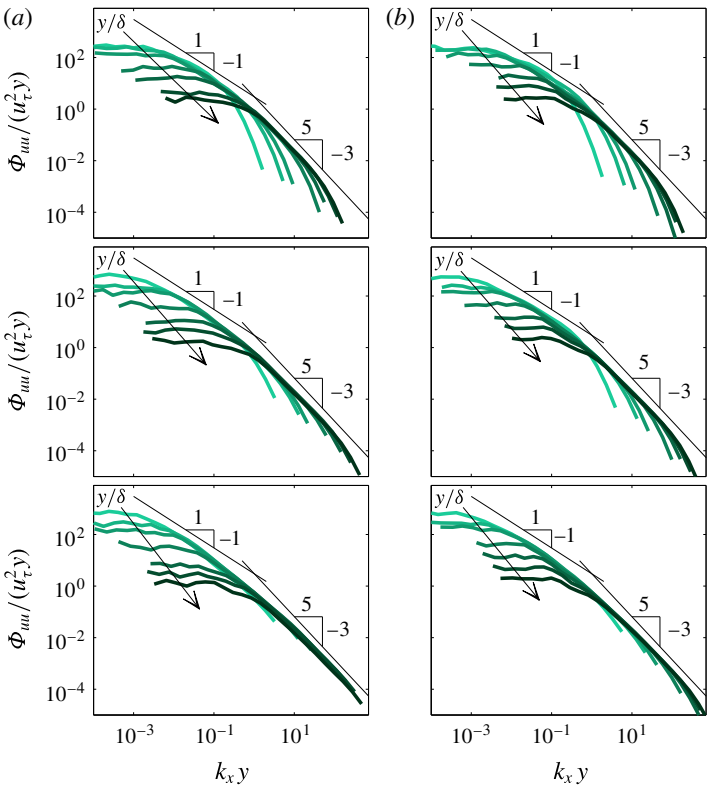

FIGURE 4. (Colour online) Spectra in wall scaling for boundary layer (*a*) and pipe flow (*b*) at wall-normal positions $y/\delta \approx 0.001$, 0.005, 0.01, 0.05, 0.15, 0.3 and 0.5, for $Re_\tau \approx 5 \times 10^3$, 20×10^3 and 70×10^3. Arrow indicates increasing y/δ.

The two Reynolds number cases shown in figures 5 and 6 demonstrate a reasonable collapse at lower wavenumbers in outer scaling (δ), and at higher wavenumbers in wall-normal scaling (y), especially in the turbulent wall layer. However, no region exists where both scalings collapse the data simultaneously, as noted previously by Morrison *et al.* (2004) and Rosenberg *et al.* (2013) for pipe flow. Although a small plateau region may be present around $y/\delta = 0.15$, this behaviour disappears at points either closer to the wall, or further away. This plateau, its extent and its variation with Reynolds numbers is further discussed in § 5. Similar trends can be observed in the spectra with varying Reynolds number at different wall-normal locations, as in figure 7.

Morrison *et al.* (2004) suggested that the lack of overlap in the scaling of the spectra may happen if u_τ is not the appropriate velocity scale for outer scaling. Also, del Álamo *et al.* (2004) suggested that the large wall-attached motions do not scale with u_τ because their contribution to the Reynolds stress is limited by the impermeability of the wall. They proposed a logarithmic correction to the k_x^{-1} spectrum given by $k_x \Phi_{uu} = \beta u_\tau^2 \log(2\pi\alpha^2/(k_x y))$, and with $\alpha = 2$ and $\beta = 0.2$ the correction agreed well with experimental and numerical spectra in the range $y < \lambda_x < 10y$ ($0.63 < k_x y < 6.3$). We see from figure 5 that for $Re_\tau = 5000$ in pipe flow a small interval in wavenumber agrees with this relation over the suggested bounds $0.63 < k_x y < 6.3$, but the boundary layer spectra seem to have a different

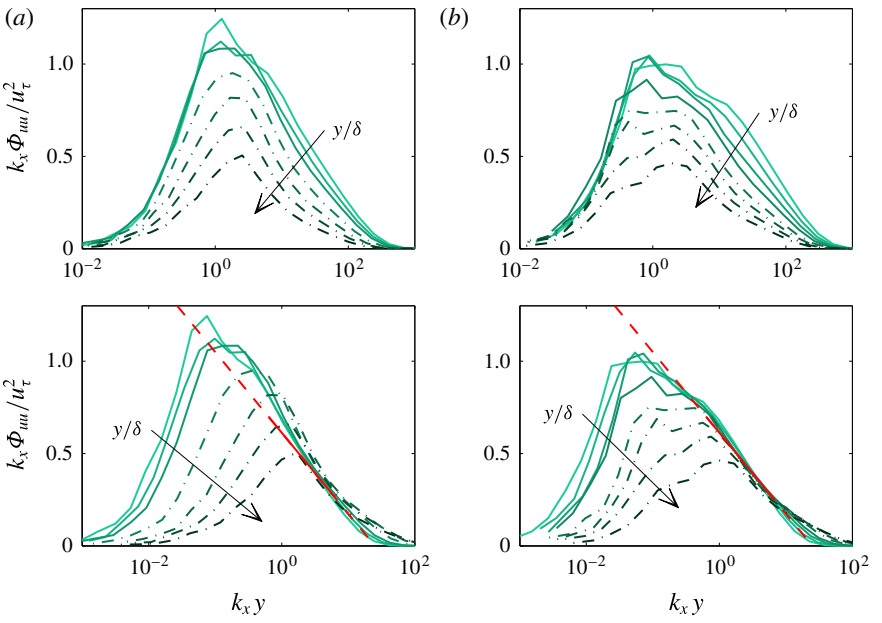

FIGURE 5. (Colour online) Premultiplied spectra for boundary layer (*a*) and pipe flow (*b*) at $Re_\tau \approx 5 \times 10^3$ with varying y/δ; ——, turbulent wall region ($200/Re_\tau < y/\delta < 0.15$); – · – · –, wake region ($0.15 < y/\delta < 0.7$); arrow indicates increasing y/δ; – – – – –, relation proposed by del Álamo *et al.* (2004), shown as solid line for $0.63 < k_x y < 6.3$.

slope. At $Re_\tau = 70\,000$ (figure 6), this relation agrees with the data over a wider range than that suggested by del Álamo *et al.* (2004), but for the boundary layer the slope β may depend on Reynolds number ($\beta = 0.23$ and 0.19 were better fits for $Re_\tau = 5000$ and 70 000, respectively). These observations provide some support for the suggestion that u_τ may not be the correct velocity scale for large scales, which infers that complete similarity (and the k_x^{-1} region) cannot be expected to occur even at very high Reynolds numbers.

Hence, it appears that in boundary layer and pipe flows in the turbulent wall region there is no obvious k_x^{-1} region that persists with Reynolds number, or with a change in wall-normal location, and the spectra do not exhibit a region that collapses both in inner and outer scaling. This brings into question the relationship between the spectral overlap arguments of Perry & Abell (1977) and Perry *et al.* (1986) and the logarithmic variation of the variances. This point is further discussed in § 5.

3.3. *Scaling of spectral peaks in wavenumber space*

In pipe flow, Rosenberg *et al.* (2013) identified distinct Reynolds number independent scaling for the wavenumber location of the LSM and VLSM peaks in each wall-normal region. Near the wall at $y^+ < 12$, a single peak was present at a wavenumber that scaled with y, where $k_x y \approx 0.07$. At $y^+ = 12$, the low- and high-wavenumber loci bifurcated, where the location of the LSM peak scaled with the viscous length ν/u_τ ($k_x^+ \approx 0.006$) over the range $12 < y^+ < 67$, and then for $y^+ > 67$ its location scaled with y according to $k_x y \approx 0.4$ up until $y/\delta = 0.15$. Beyond $y/\delta = 0.15$, the LSM peak location scaled with δ according to $k_x \delta = 2.6$.

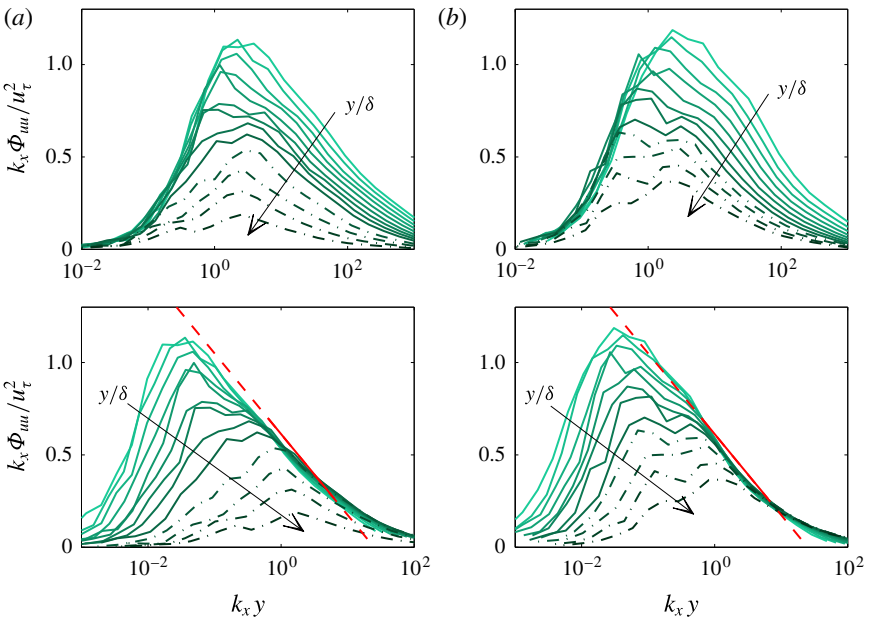

FIGURE 6. (Colour online) Premultiplied spectra for boundary layer (*a*) and pipe flow (*b*) at $Re_\tau \approx 70\,000$ with varying y/δ; ——, turbulent wall region ($800/Re_\tau < y/\delta < 0.15$); –·–·–, wake region ($0.15 < y/\delta < 0.7$); arrow indicates increasing y/δ; – – – – –, relation proposed by del Álamo *et al.* (2004), shown as solid line for $0.63 < k_x y < 6.3$.

As to the VLSM peak, Rosenberg *et al.* (2013) found that, somewhat surprisingly, its location also scaled with wall-normal distance y in the turbulent wall region ($k_x y \approx 0.045$), and not with δ as seen for the SS peak in boundary layers by Hutchins & Marusic (2007). Rosenberg *et al.*'s (2013) analysis for pipe flow was repeated here using every wall-normal location (the original study used only about a third of the data), and it was found that for $y^+ > 50$ the VLSM peak location was better described by $k_x\delta \approx 0.17\,(\delta/y)^{0.67}$, that is, it is more precise to say that the VLSM peak in the turbulent wall region in pipes follows a weak mixed scaling rather than a simple wall-normal scaling. Finally, for $y/\delta > 0.15$ the location of the VLSM peak scaled as $k_x\delta \approx 0.45$.

Here, we apply the methodology used by Rosenberg *et al.* (2013) to find the location of the spectral peaks in the boundary layer. To estimate the wavenumber peak location, a Gaussian curve in $\log k_x$ was locally fitted to the data. At locations where the LSM peak was more difficult to identify, because it appeared more as a narrow shoulder rather than as a distinct peak (in the region $100 < y^+ < 0.15$), a cubic spline was used to fit the data and the point of inflection was taken as an estimate of the peak location.

The results are shown in figures 8 and 9 in inner and outer variables, respectively. In the near-wall region, for $y^+ < 10$, a single peak is observed, scaling with the wall-normal distance and located at about $k_x y \approx 0.05$ ($\lambda_x \approx 125y$). This scaling is the result of the local mean velocity used as convection velocity when applying Taylor's hypothesis. If no Taylor hypothesis were applied, the inner peak scales simply with the viscous time scale, being constant at $f^+ = f\nu/u_\tau^2 \approx 0.008$ or $t^+ = 1/f^+ \approx 125$.

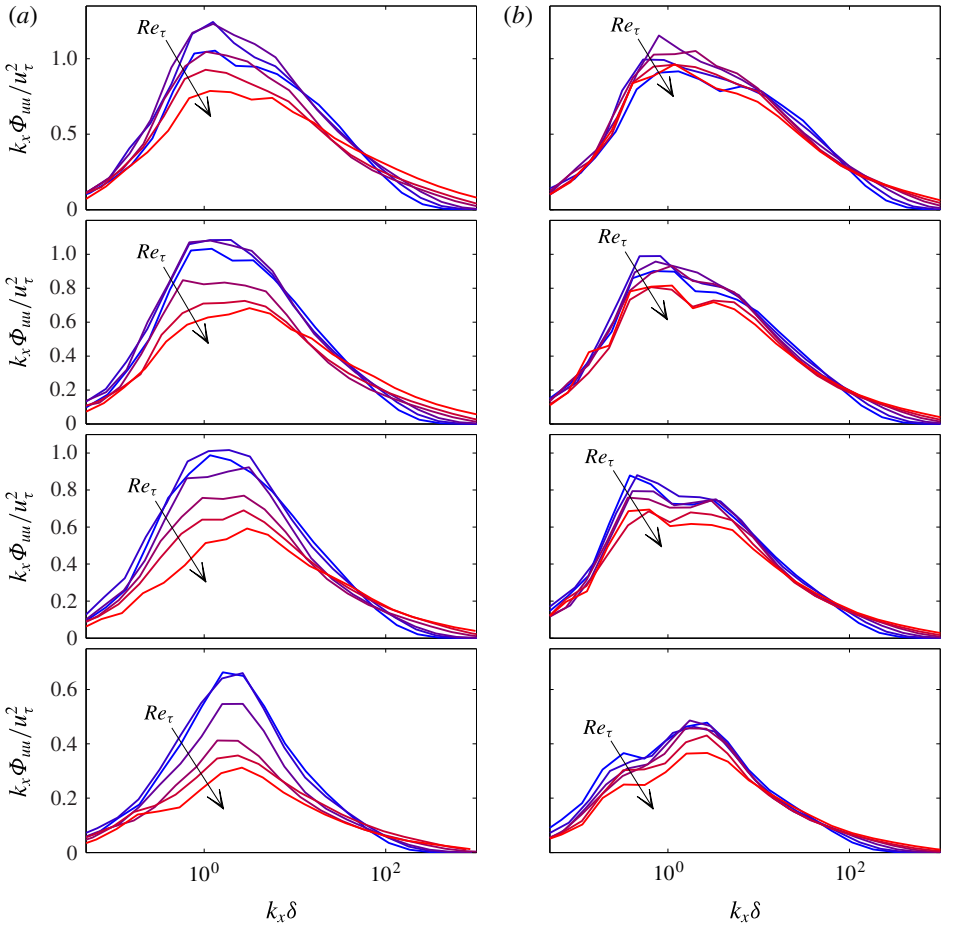

FIGURE 7. (Colour online) Premultiplied spectra for boundary layer (*a*) and pipe flow (*b*) at wall-normal locations $y/\delta = 0.05$, 0.1, 0.15 and 0.5. Arrow indicates increasing Re_τ from 3000 to 70 000 (as line color changes from blue to red in online version).

Near $y^+ \approx 10$, close to where the inner peak in the variance is located, there is a bifurcation in the loci of the peaks, so that the peaks associated with the LSM begin to follow $k_x^+ \approx 0.005$ (or $\lambda_x \approx 1250\eta$). For $50 < y^+ < 0.15Re_\tau$, the location of the LSM peak scales with y as $k_x y \approx 0.4$. The location of the SS peak in the same region seems to follow $k_x\delta \approx 0.33(\delta/y)^{0.5}$, showing simultaneous dependence on wall-normal distance and the boundary layer thickness, as it did in pipe flow. This trend, when expressed in terms of the wavelength, gives $\lambda_x^+ \approx 20\,(y^+Re_\tau)^{0.5}$, which suggests that in the region $50 \lesssim y^+ \lesssim 0.15Re_\tau$ the SS are associated with wavelengths $\lambda_x \sim (y\delta)^{0.5}$. At first sight, this result is consistent with the observations of Morrill-Winter & Klewicki (2013) who found that the wall-normal intensities begin scaling with $\sqrt{Re_\tau}$ near $y^+ \approx C\sqrt{Re_\tau}$. However, the implications and the consequences of this consistency are unclear, as it will be shown later that the location of the peak in the spectra in the streamwise velocity component does not appear to scale as $\sqrt{Re_\tau}$ across the range of Reynolds numbers considered here. In the outer region, for $y/\delta > 0.15$, the SS peak is no longer evident and only the LSM peak survives, with its location scaling as $k_x\delta \approx 2$. This value corresponds to $\lambda_x \approx 3\delta$, as found by Guala *et al.* (2006).

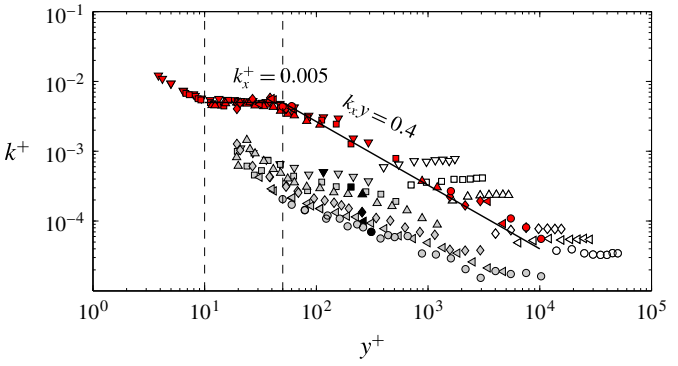

FIGURE 8. (Colour online) Spectral peak locations in inner coordinates for the boundary layer. Filled (red online) symbols: near-wall and LSM peaks. Open symbols: peak locations for $y/\delta > 0.15$. Filled grey symbols: SS peaks. Filled black symbols: outer spectral peak location. Other symbols as in table 1. ––––, $y^+ = 10$ and $y^+ = 50$.

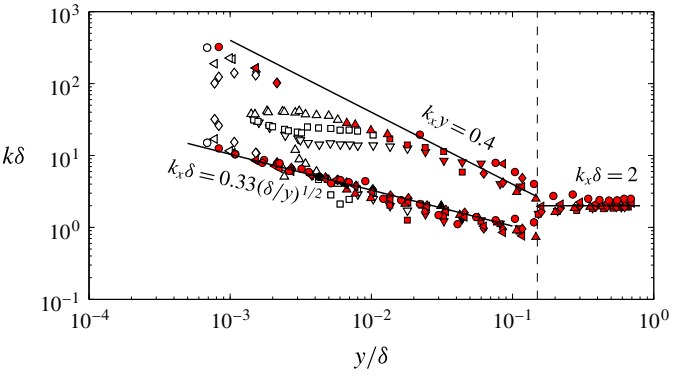

FIGURE 9. (Colour online) Spectral peak locations in outer coordinates for the boundary layer. Filled (red online) symbols: all peaks in region $50 < y^+ < 0.15Re_\tau$. Open symbols: peaks for $y^+ < 50$. Filled black symbols: outer spectral peak location. Other symbols as in table 1. – – – – –, $y/\delta = 0.15$.

Overall, it appears that the LSMs have similar characteristics in boundary layer and pipe flows, although the SSs and VLSMs display some differences, even at very high Reynolds numbers; in outer variables the trajectory of the peak for boundary layers varies as $(\delta/y)^{0.5}$, whereas for pipes it varies as $(\delta/y)^{0.67}$. In addition, the outer flow in the pipe continues to be characterized by LSMs and VLSMs, whereas in the boundary layer only a single peak associated with the LSM is present, suggesting that the SS organization is lost in the wake region.

3.4. *Scaling of outer spectral peak*

Here, we consider the scaling of the outer spectral peak in the region of turbulent wall flow ($50 \lesssim y^+ \lesssim 0.15Re_\tau$). Recall that the outer spectral peak is the point where the VLSM or SS spectral peak has its maximum magnitude $(k_x\Phi_{uu})_{OSP}$, and it is described by a specific physical location y_{OSP} and wavenumber k_{OSP}. In boundary layers, Hutchins & Marusic (2007) and Mathis *et al.* (2009) found that the location

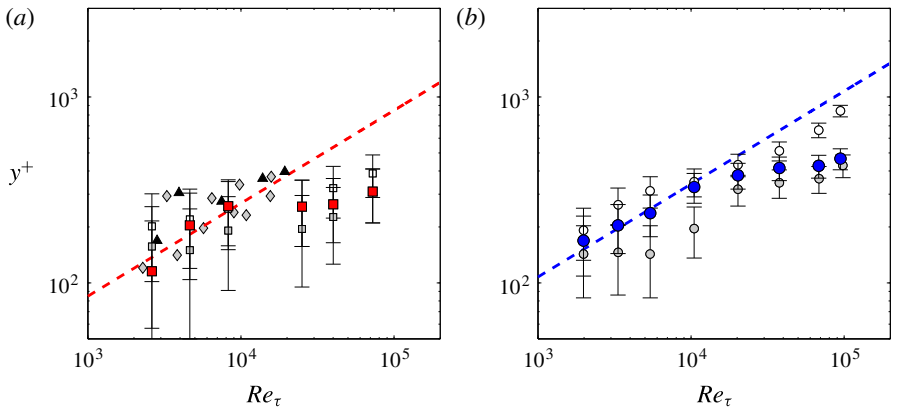

FIGURE 10. (Colour online) Wall-normal location of outer spectral peak for boundary layer (*a*) and pipe flow with all data from Hultmark *et al.* (2012) (*b*). ■, boundary layer with error bounds $\Delta y^+ = \pm 100$; ●, pipe with error bounds $\Delta y^+ = \pm 60$; (– – – – –), $y^+ = 2.68Re_\tau^{0.5}$; (– – – – –), $y^+ = 3.40Re_\tau^{0.5}$; □, $R_m = 0$ location for boundary layer; ○, $R_m = 0$ location for pipe; ▲, $R_m = 0$ location for boundary layer from Mathis *et al.* (2009); ■, location of outer peak in u^{2+} for boundary layer; ●, location of outer peak in u^{2+} for pipe; ◆, skewness zero crossing location from Vincenti *et al.* (2013).

of the outer spectral peak in inner variables, as well as its magnitude, varied with Reynolds number.

For the current boundary layer study, the locations of the outer spectral peak in $[y_{OSP},\ k_{OSP}]$ coordinates are shown by the black symbols in figures 8 and 9. Each location was found by locally fitting a Gaussian curve to the data and then nominating the closest available data point as y_{OSP}. The variation of y^+_{OSP} with Reynolds number is shown in Figure 10(*a*). The data were acquired in Δy^+ increments of about 40–100, and the location of the peak therefore has a comparable uncertainty range (the error bars show uncertainty limits of $\Delta y^+ \pm 100$). As can be seen, the locations of the outer spectral peak in the boundary layer at lower Reynolds numbers follow $Re_\tau^{0.5}$ trend (dashed line shows best fit for $Re_\tau < 20\,000$), but at higher Re_τ the trend is much weaker. In fact, for $Re_\tau \gtrsim 20\,000$, its location seems to remain approximately fixed at $y^+ \approx 300$.

To compare these observations to those of Mathis *et al.* (2009), consider now the amplitude modulation correlation coefficient R_m, representing the degree of modulation of the small-scale fluctuations by the large energetic scale motions. Mathis *et al.* found that where $R_m = 0$, that is, the location of the point where LSMs and small-scale motions are not correlated, seemed to correspond closely with the location of the outer spectral peak. The loci of these zero crossings are shown in figure 10 together with the $R_m = 0$ locations found for the current data set, using a cutoff frequency $f^+ = 0.005$ for the boundary layer and 0.002 for the pipe. Also shown are the locations of the outer peak in the variances for current data, which mark approximately the point where the variances begin to follow a logarithmic behaviour (Vallikivi *et al.* 2015), and the skewness zero crossing locations from Vincenti *et al.* (2013), a point that has also been observed to behave in similar manner to the peak in the spectra and variances. We see that all indicators follow a similar trend to the outer spectral peak location up to $Re_\tau \approx 20\,000$, but the higher-Reynolds-number data all show a much slower rate of increase.

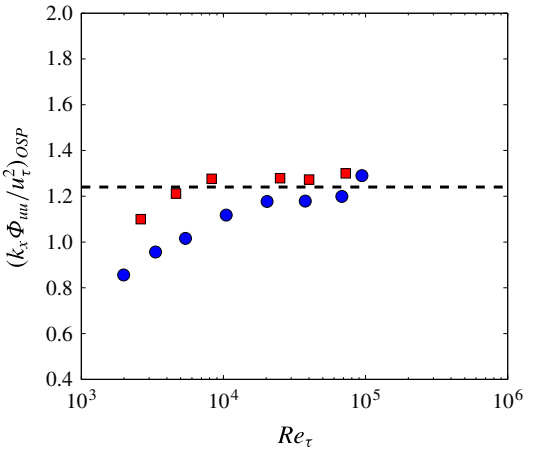

FIGURE 11. (Colour online) Magnitude of the outer spectral peak: ■, boundary layer; ●, pipe; −−−−−, $k_x\Phi_{uu}/u_\tau^2 = 1.24$.

For the pipe, the outer spectral peak behaves in a similar manner to that in the boundary layer (see figure 10*b*), but its location shows less variation, probably because the pipe data are available in smaller increments ($\Delta y^+ \approx 30$–60), allowing for higher precision. Again, the lower-Reynolds-number range seems to agree well with $Re_\tau^{0.5}$ trend (dashed line shows best fit for $Re_\tau \lesssim 20\,000$), but at higher Re_τ the data show a slower increase in y^+. Just as in boundary layers, for $Re_\tau \gtrsim 20\,000$ its location seems to remain approximately fixed, this time at $y^+ \approx 400$. This behaviour is shared by the location of the peak in u^{2+}, but in contrast the $R_m = 0$ location for the pipe continues to increase with Reynolds number, something not seen in the boundary layer data.

The magnitude of the outer spectral peak for each case is shown in figure 11. For both flows, the amplitude appears to approach a constant value at high Reynolds numbers where $k_x\Phi_{uu}/u_\tau^2 \approx 1.24 \pm 0.05$, although the rate of approach is faster for the boundary layer. These observations and the significance of the value 1.24 will be discussed in more detail below, but we should note that there are considerable uncertainties in finding the magnitude of the peak (principally due to calibration issues and the difficulties in finding the friction velocity in boundary layers).

The wavenumber associated with the outer spectral peak, k_{OSP}, is shown in figure 12. For increasing Reynolds number, it decreases in viscous units as $k_{OSP}^+ \approx MRe_\tau^{-0.5}$, while increasing in outer scaling as $k_{OSP}\delta \approx MRe_\tau^{0.5}$, where $M = 0.2$. In terms of wavelength, this gives $\lambda_{OSP}^+ \approx (M/2\pi)Re_\tau^{0.5}$ and $\lambda_{OSP}/\delta \approx (M/2\pi)Re_\tau^{-0.5}$, respectively, suggesting that the wavelength associated with the large energetic scales neither scales with the inner length scale, nor with the outer length scale; λ_{OSP} appears to emerge as an independent length scale. In addition, $\lambda_{OSP} \approx (M/2\pi)(\delta\nu/u_\tau)^{0.5}$, so that at very large Reynolds numbers $\nu/u_\tau \ll \lambda_{OSP} \ll \delta$.

The wavenumber of the outer spectral peak appears, therefore, to be a new scale representative of the log region. Vassilicos *et al.* (2014) recently suggested that for the Townsend–Perry attached eddy model to show the correct behaviour for the integral length scale at high Reynolds number, an additional length scale needs to appear, one that lies between the inner and outer scales. Our current observations are closely aligned with that proposal. In addition, the appearance of a new region described by the length scale λ_{OSP} is consistent with the observation of Vallikivi *et al.* (2015)

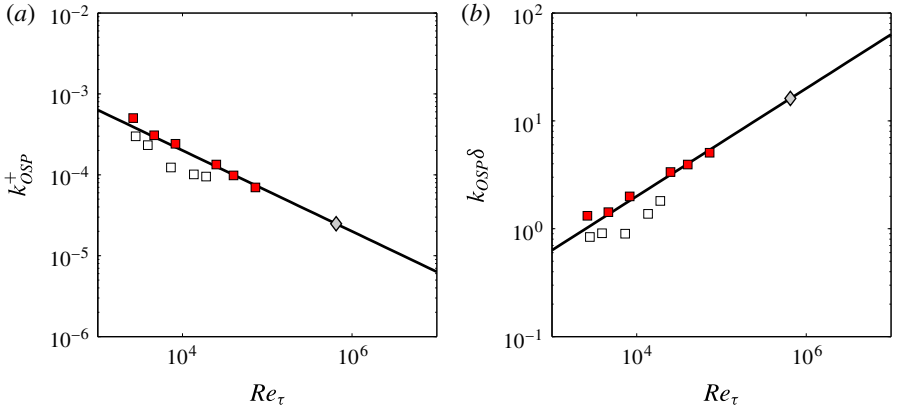

FIGURE 12. (Colour online) Wavenumber of the outer spectral peak in inner (*a*) and outer coordinates (*b*): ■, boundary layer (uncertainty in k^+_{OSP} is about $\pm 50\,\%$; □, boundary layer data from Mathis *et al.* (2009); (solid line), $k_x^+ = 0.02Re_\tau^{-0.5}$ (*a*); $k_x\delta = 0.02Re_\tau^{0.5}$ (*b*); ◇, predicted wavenumber for $Re_\tau = 650\,000$.

who find a log region (in mean and intensity) only after the outer spectral peak has emerged.

Given the consensus in the literature that the outer spectral peak is associated with the SS, there are two potential ways to interpret the above observations. First, we could say that the SS are actually the manifestation of this region in the flow, rather than the largest scales of motion. This would lead to a rather startling implication that at lower Reynolds numbers the SS appear as very large scales (that is, $\lambda_x/\delta \approx 3$–$6$) due to a lack of scale separation, but at higher Reynolds numbers the length scale of the SS decreases. The length scale associated with the outer spectral peak in an atmospheric boundary layer at $Re_\tau \approx 650\,000$ is expected to be $\lambda_x/\delta \approx 0.4$ (as inferred from the correlation shown in figure 12), which is much smaller than the scales of the VLSM/SS. This suggests that this first interpretation is too stringent and may not truly represent the data.

An alternate and perhaps more suitable interpretation is that there is a need to decouple the scale and location of the outer spectral peak from that of the SS/VLSMs. It can be seen from the spectra that, although the OSP appears to move towards the wall and become smaller (in outer scaling) with increasing Reynolds number, there is still significant energy content in larger scales. Therefore, the SS (in boundary layers) and VLSMs (in pipes) continue to be dynamically relevant. This means that the wavelength of the outer spectral peak is in fact a new length scale that emerges in parallel with the VLSMs. The VLSMs start to appear at 'lower' Reynolds numbers (say $Re_\tau \approx 2000$), but this new length scale only emerges when there is sufficient scale separation even beyond the one required for the VLSMs ($Re_\tau > 20\,000$). At these higher Reynolds numbers, the VLSMs represent the plateau region in the spectra (instead of the peak) while the peak itself captures this new inertial length scale.

To show that there is at least some support for this notion at even higher Reynolds numbers, figure 13 reproduces the spectrogram obtained in the neutral atmospheric boundary layer by Mathis *et al.* (2009), where we see that there may indeed be an outer spectral peak whose location is proportional to $\ln Re_\tau$ and whose wavelength (in outer units) follows $Re_\tau^{-0.5}$. The location and the wavelength of this prediction appears

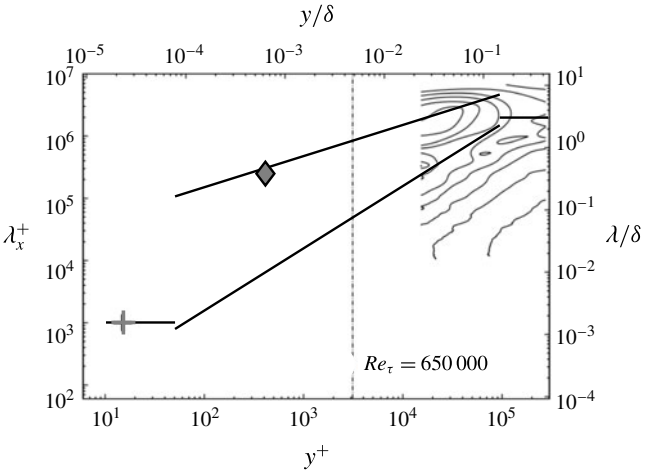

FIGURE 13. Contour plot of the spectra in the atmospheric boundary layer at $Re_\tau = 650\,000$, adapted from Mathis *et al.* (2009): +, location of inner spectral peak; ◆, speculated location of outer spectral peak; (solid lines), trends in the loci of LSM and SS peaks as described in § 3.3.

to be consistent with the peak found by Guala, Metzger & McKeon (2011) in the wall-normal range $y^+ \approx 1000$ at a wavelength of about 0.45δ. Note that these values have been inferred from figure 12 in Guala *et al.* (2011) that shows multiple peaks at different wall-normal locations and wavenumbers and the uncertainty in identifying a peak in the spectrogram (in wall-normal location) is stated to be about ± 1000 wall-units.

As noted earlier, pipe flows behave somewhat differently. Here, we expect that $\lambda_{OSP}/\delta \propto Re_\tau^{-0.67}$ and $\lambda_{OSP}^+ \propto Re_\tau^{0.33}$. Hence, the scale separation between inner and inertial ranges appears slower in pipes than in boundary layers, whereas the separation between outer and inertial scales is faster. The slower approach to the inner limit agrees well with the observation that the appearance of a logarithmic region occurs at a higher value of y^+ in pipes than in boundary layers.

4. The mesolayer

We now draw together the observations on the spectral peaks and the behaviour of the mean velocity and the variances. To this end, contour maps of the premultiplied spectra in the boundary layer and pipe are shown in figures 14 and 15, together with the corresponding mean velocity and variance profiles. We see again that the location of the outer spectral peak given by the correlations of Hutchins & Marusic (2007) and Mathis *et al.* (2009) for boundary layers overestimate its Reynolds number dependence. In addition, the location of the outer spectral peak coincides closely with the start of the logarithmic regions in the mean velocity and the variance. The overall behaviour of the spectra in pipe flow is very similar to that in boundary layers, in that the inner spectral peak stays approximately constant in viscous units and the outer spectral peak is identified with the start of the log layer, although it is located at slightly higher values of y^+ in pipes compared with boundary layers.

Based on these observations, we first identify regions I and II in figures 14 and 15, where the spectra and the statistics scale with inner variables (corresponding to the

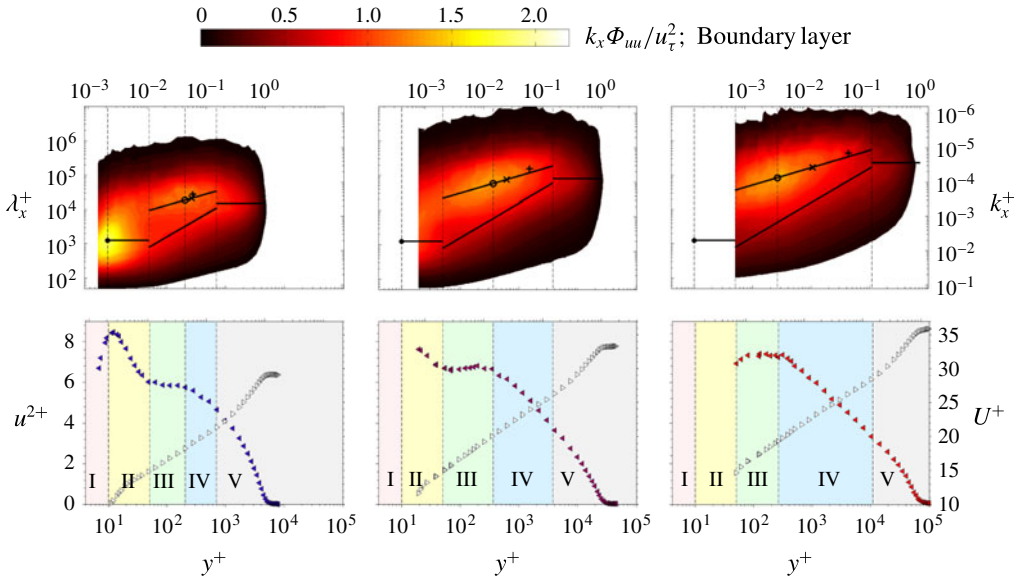

FIGURE 14. Contour plots of spectra in the boundary layer at $Re_\tau = 5 \times 10^3$, 20×10^3 and 70×10^3. Lines show trends in the loci of peaks shown in figures 8 and 9; (dashed lines), $y^+ = 10$, 50, y^+_{OSP}, $0.15Re_\tau$; ●, location of near-wall spectral peak. Location of outer spectral peak: ○, current data; ×, Mathis *et al.* (2009); +, Hutchins & Marusic (2007).

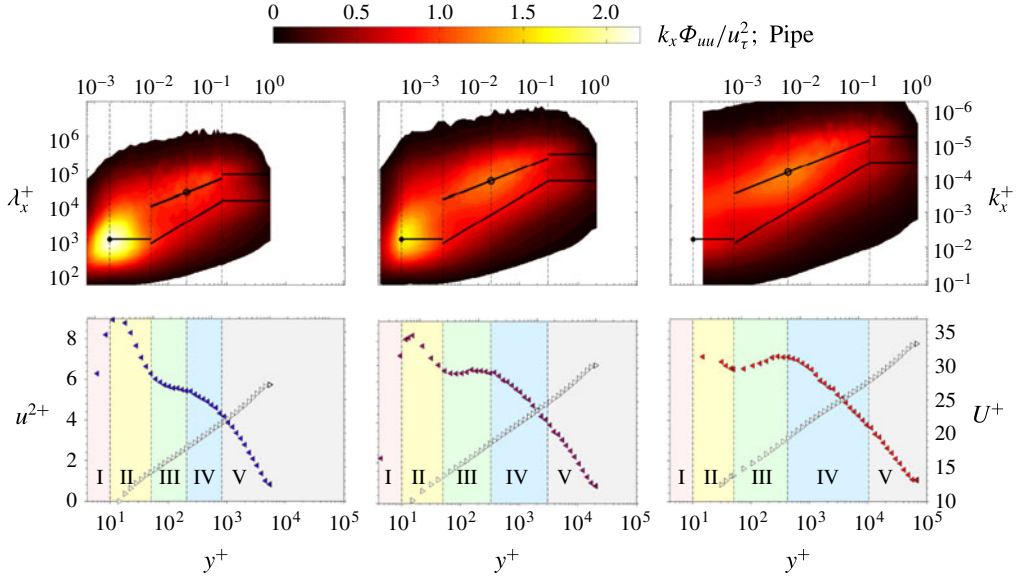

FIGURE 15. Contour plots of spectra in the pipe at $Re_\tau = 5 \times 10^3$, 20×10^3 and 70×10^3. Lines show trends in the loci of peaks shown in figures 8 and 9; (dashed lines), $y^+ = 10$, 67, y^+_{OSP}, $0.15Re_\tau$; ●, location of near-wall spectral peak; ○, location of outer spectral peak.

linear sublayer and the buffer layer). We also recognize a region IV where the mean velocity and variances follow a log-law, marked approximately at its inner boundary by the location of the outer spectral peak, and at its outer boundary by the point where $y/\delta = 0.15$. In between, there is region III where a Reynolds-number-dependent behaviour can be seen in all parameters, which we identify as the mesolayer.

The term mesolayer was initially introduced by Long & Chen (1981), but found a clearer expression in the work of Afzal (1982), Afzal (1984), Sreenivasan & Sahay (1997), George & Castillo (1997), Wosnik, Castillo & George (2000) and Wei *et al.* (2005). With the exceptions of George & Castillo (1997) and Wosnik *et al.* (2000), who argued that the mesolayer is a region where energy dissipation scales with $\nu u^2/y^2$ rather than u^3/y so that a Reynolds number dependence is retained in the scaled Reynolds stress and mean flow equations, all other studies rely on the presence of an emerging intermediate wall-normal length scale that increases as $\sqrt{Re_\tau}$. For example, Afzal (1982) used asymptotic expansions together with an integrated momentum equation to show the emergence of a mesolayer whose location scales as $\sqrt{Re_\tau}$ in pipe flow. Sreenivasan & Sahay (1997) found that the location of the peak in Reynolds shear stress ($\langle -uv \rangle^+$) scales as $\sqrt{Re_\tau}$, and expanded the once integrated form of the momentum equation about this peak to determine the extent of the mesolayer. Finally, Wei *et al.* (2005), by examining the mean momentum balance in wall-bounded turbulent flows, identified the mesolayer (layer III in their nomenclature) as a region where there is a balance between turbulent inertia (stress gradients), the viscous force, and either the force due to the pressure gradient in pipes or the mean advection in boundary layers. They identified the extent of the mesolayer, and using the data available at the time verified its outer limit to be $O(\sqrt{Re_\tau})$ in all flows. A summary description of the different layers and their extent is given by Klewicki (2013*b*).

The current data show a region akin to the above-mentioned mesolayer for the mean flow, the variances and the spectra, but the bounds are different from those determined in previous studies. In the premultiplied spectra, this is the region for $y^+ > 50$ (for the boundary layer) and $y^+ > 67$ (for the pipe) where the LSM and VLSM/SS peaks can be identified, with these two peaks competing until the VLSM/SS peak becomes dominant. The energy associated with the VLSM/SS peak increases throughout this mesolayer, and the outer spectral peak acts as the outer bound for this region. It is seen that the location of the outer spectral peak does not appear to follow the $\sqrt{Re_\tau}$ scaling proposed for pipes and boundary layers in previous studies. Over the entire range of Reynolds numbers available, y^+_{OSP} appears to follow a much weaker scaling (perhaps as $\ln Re_\tau$) for both pipes and boundary layers. However, upon further examination, as discussed in the previous section, there appears to be two different trends over the range of Reynolds numbers explored here. For Reynolds numbers up to about 20 000, $y^+_{OSP} \propto \sqrt{Re_\tau}$, whereas for higher Reynolds numbers, y^+_{OSP} appears to be a constant (to within experimental uncertainty).

It is important to note that previous analytical studies determined the bounds of the mesolayer based on the peak in Reynolds shear stress and not on the location of the outer spectral peak. In fact, Chin *et al.* (2014) recently calculated the Reynolds shear stress distribution using the mean profiles from Hultmark *et al.* (2013) and found that the peak in Reynolds shear stress follows $\sqrt{Re_\tau}$ scaling. However, this location does not match the location of the outer spectral peak as determined here using the same data. To the best of the authors' knowledge, there is no particular reason for the two locations to exhibit the same Reynolds number scaling. Up to a certain Reynolds number (say, $Re_\tau \approx 20\,000$), these two locations appear to be close to each other, or

at least within the error bars on our data, and the location of the outer spectral peak can be used as a proxy for the location of the Reynolds shear stress peak. For much higher Reynolds numbers, we need additional data to confirm that this correspondence continues to hold true. Therefore, the mesolayer described in the current work may not be the same as those in the other studies that rely on arguments on the Reynolds shear stress distribution.

Finally, it is interesting to note that the streamwise length scale, inferred using Taylor's hypothesis, associated with the outer spectral peak appears as an intermediate length scale that seems to scale with $\sqrt{Re_\tau}$ in both pipes and boundary layers. We therefore suggest that the mesolayer may be identified with the emergence of this new streamwise length scale. This observation differs from previous work where the focus was on the emergence of a new wall-normal length scale. Further work is required to understand the emergence of this length scale and how it might be associated with the mesolayer scaling described in other studies.

5. The log-layer

For boundary layers and pipes, we saw that at a sufficiently high Reynolds number the location of the outer spectral peak appears to be either fixed or slowly varying in inner scaling, and its magnitude appears to asymptote to a constant value of about 1.24 ± 0.05 (figure 11). The spectrograms shown in figures 14 and 15 demonstrate that the location of the outer spectral peak at high Reynolds numbers marks the start of a broad plateau where, at any given wall-normal location $k_x\Phi_{uu}/u_\tau^2 \approx A_1'$, that is, $\Phi_{uu}(k_x y)/u_\tau^2 \approx A_1'/(k_x y)$. At any given Reynolds number, this plateau extends approximately from a low-wavenumber limit given by a fixed value of $k_x\delta = F$ to a high-wavenumber limit given by $k_x y = 0.4$. Hence, by integrating the spectrum over this plateau we find a very similar result to that given by (1.2), namely,

$$u^{2+} = \frac{1}{u_\tau^2}\int_{Fy/\delta}^{0.4} \Phi_{uu}(k_x y)\mathrm{d}(k_x y) = B_1' - A_1' \ln\left[\frac{y}{\delta}\right]. \tag{5.1}$$

The value of $A_1' \approx 1$, and so it is generally smaller than A_1, and it may also be a weak function of y/δ. Nevertheless, we can derive a logarithmic region in the variances with a slope that is close to the asymptotic value of the outer spectral peak, without requiring an overlap region, providing the lower-wavenumber part of the spectrum scales with δ, the higher-wavenumber part scales with y, and A_1' does not depend strongly on y/δ. Note that the integral of the spectrum is likely to be reasonably insensitive to the details of the spectral distribution, so that the underlying physical arguments, especially the attached eddy hypothesis, retain an important role. In this respect, an alternative theoretical approach was recently suggested by Hultmark (2012), who showed a logarithmic behaviour in variances without involving spectral arguments and therefore independent of any k_x^{-1} region in the spectrum.

These observations suggest that the essential condition to observe a logarithmic behaviour in the variances is a plateau region defined by a sufficient scale separation between y_{OSP}^+ and $y/\delta = 0.15$. However, the extent of the approximate plateau in the spectrum between $k_x\delta = F$ and $k_x y = 0.4$ depends upon the wavenumber of the outer spectral peak. Since $k_{OSP}\delta$ increases and k_{OSP}^+ decreases with increasing Re_τ, we expect that a plateau (whose value is near 1.24) will emerge over a large range of wavenumbers and wall-normal locations at Reynolds numbers where $\nu/u_\tau \ll \lambda_{OSP} \ll \delta$. These conditions are consistent with those necessary to have λ_{OSP} emerge as a scale representative of the log-layer.

6. Conclusions

Streamwise turbulent spectra for Reynolds numbers in the range $2600 \lesssim Re_\tau \lesssim 72\,500$ were studied in boundary layer flows, and compared with data at similar Reynolds numbers taken previously in pipe flows. In the high-wavenumber (low-wavelength) region, all spectra in both flows showed an excellent collapse in Kolmogorov scaling with a slope approaching (but not reaching) $k_x^{-5/3}$ for increasing wall-normal distance and Reynolds number. This observation is in agreement with the theory of Mydlarski & Warhaft (1996), Gamard & George (2000) and others, on the slow asymptotic behaviour of the exponent toward $-5/3$.

At intermediate wavelengths, the spectra were found to scale well with y, and at large wavelengths the spectra scaled with the outer length scale δ. However, in contrast to the predictions by Perry *et al.* (1986), no region of overlap of these scalings was seen, as first noted by Morrison *et al.* (2004).

For boundary layers, the near-wall inner spectral peak in the premultiplied spectrum followed $t^+ \approx 125$ for $y^+ \lesssim 10$. At $y^+ \approx 10$, the loci bifurcated so that the LSM peak first followed $k_x^+ \approx 0.005$ and then $k_x y \approx 0.4$, in close agreement with previous findings in pipe flow. After bifurcation, a peak associated with SS emerged, scaling with outer variables and following $\lambda_x^+ \approx 20(y^+ Re_\tau)^{0.5}$ for $50 \lesssim y^+ \lesssim 0.15 Re_\tau$. Outside the logarithmic layer above $y/\delta > 0.15$, the peaks associated with SS and LSM merged into one peak located at about $\lambda_x \approx 3\delta$. This is in contrast to pipe flows, where the two peaks remain distinct.

The location of the outer spectral peak increased as $\sqrt{Re_\tau}$ up to a $Re_\tau \approx 20\,000$ and beyond that the trend was much weaker and seemed to approach a constant value, suggesting that the physical region containing most of the turbulent energy is getting smaller and moving closer to the wall (in physical units).

In boundary layers and pipes, the wavelength of the outer spectral peak appeared to increase with Reynolds number using inner scaling and decrease with Reynolds number using outer scaling, so that the scales associated with the outer spectral peak decrease in size relative to the large scales with increasing Reynolds number. It is possible, therefore, that the wavelength of the outer spectral peak is a representative scale of the inertial range where $\nu/u_\tau \ll \lambda_{OSP} \ll \delta$. At high Reynolds numbers, the location of the outer spectral peak y_{OSP} marks the start of a broad plateau in the premultiplied spectrum that gives the appearance of a k_x^{-1} region. The extent of the plateau depends upon satisfying $\nu/u_\tau \ll \lambda_{OSP} \ll \delta$. By integrating the spectrum over the plateau region, we derive a logarithmic region in the variances with a slope that is close to the value of 1.24, as was found to exist in pipes and boundary layers by Hultmark *et al.* (2012), Hultmark *et al.* (2013), Marusic *et al.* (2013) and Vallikivi *et al.* (2015). Hence, the log-layer in wall-bounded flows seems directly associated with the appearance of an outer spectral peak whose wall-normal location scales with wall units. For the laboratory results presented here, an extensive k_x^{-1} range is not obvious due to a lack of sufficient scale separation between inner scales, outer scales and the inertial scale λ_{OSP}. This observation, however, is consistent with the presence of k_x^{-1} in even higher-Reynolds-number flows where this scale separation is present, such as in atmospheric boundary layers.

Based on the behaviour of peaks in the energy spectra, together with the results on the turbulence statistics obtained by Vallikivi *et al.* (2015), we now propose five distinct regions in wall-bounded flows:

Region I: $y^+ \lesssim 10$. Here, the near-wall structures scale as $\lambda_x/y \approx$ const. (or $t^+ \approx$ const. without using Taylor hypothesis). The inner spectral peak location corresponds to $y^+ \approx 10$ and $\lambda^+ \approx 1250$ ($k_x^+ = 0.005$), close to the location of the inner peak in the variance.

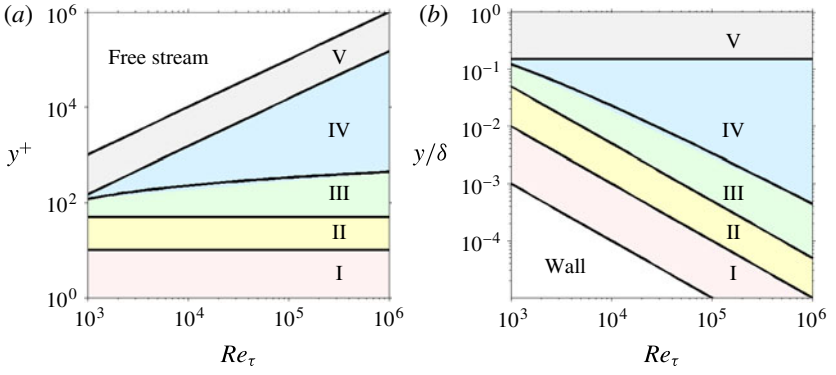

FIGURE 16. (Colour online) The extent of the principal scaling regions in boundary layers, in inner (*a*) and outer coordinates (*b*).

Region II: $10 \lesssim y^+ \lesssim 50$ (boundary layers) and 67 (pipes). Here, the near-wall structures scale as $\lambda_x^+ \approx$ const. The energy in the near-wall structures decreases and the wavelength of these structures stays about constant in viscous units at $\lambda_x^+ \approx 1250$. The decrease in the variance with increasing wall distance is matched to the decrease of the near-wall peak in the energy spectra. This region is associated with the buffer layer in the mean velocity.

Region III: 50 (boundary layers) and 67 (pipes) $\lesssim y^+ \lesssim y^+_{OSP}$. Here, $\lambda_x^+ \sim y^{+0.5} Re_\tau^{0.5}$ in boundary layers and $\lambda_x^+ \sim y^{+2/3} Re_\tau^{1/3}$ in pipes. Two energetic peaks in the spectra are present, with most of the energy associated with the SS located at $\lambda_x \sim (y\delta)^{0.5}$, and a weaker peak associated with LSMs located at about $\lambda_x \approx 20y$. The SS/VLSM peak continues to increase until y^+_{OSP} (whose limits are discussed in region IV). The variance is almost constant at lower Reynolds numbers while slightly rising at higher Reynolds numbers. In the mean velocity, the profile seems to behave as a power law in y^+. This region is associated with the mesolayer, where the mean flow is almost free of viscous effects but turbulent quantities are still affected by viscosity.

Region IV: $y^+_{OSP} \lesssim y^+ \lesssim 0.15 Re_\tau$. Here, $\lambda_x^+ \sim y^{+0.5} Re_\tau^{0.5}$ in boundary layers and $\lambda_x^+ \sim y^{+2/3} Re_\tau^{1/3}$ in pipes. The energy associated with the SS/VLSMs is decreasing and there is a logarithmic behaviour in variances. The outer spectral peak associated with SS is located where there is an outer peak in the variance. Also, y^+_{OSP} varies weakly with increasing Reynolds number (possibly following a $\ln Re_\tau$ trend over the entire range of Re_τ), contrary to previous work that indicated a stronger Reynolds number dependence (over a smaller range of Reynolds numbers). In fact, as discussed in the paper, y^+_{OSP} appears to vary as $\sqrt{Re_\tau}$ up to $Re_\tau \approx 20\,000$ and then is nearly a constant for higher Reynolds numbers. Its location coincides with the outer peak or the end of plateau seen in the variances, and therefore marks approximately the beginning of the logarithmic behaviour in the variances. The wavelength of the outer spectral peak emerges as a possible length scale for this region. The magnitude of OSP reaches a constant value, and so marks the start of a k_x^{-1} plateau that translates to a logarithmic region in the variances.

Region V: $y/\delta \gtrsim 0.15$. Here, the LSMs (and VLSMs in pipe) scale with the outer length scale. In boundary layers, the SS peak disappears, and only the LSM peak remains, showing up as a single peak associated with large-scale structures with $\lambda_x \approx$

3δ. In pipe flows, both the LSM and VLSM peaks continue to be present, scaling on δ and differing only in length. The turbulent fluctuations diminish and the mean velocity follows a Reynolds-number_independent wake function.

The extent of these regions with varying Reynolds number is illustrated in figure 16. It is clear that regions IV and V will constitute almost the full physical extent of wall-bounded flows at very high Reynolds number.

Acknowledgements

The authors would to thank W. K. George and I. Marusic for insightful discussions and suggestions, and J. Klewicki for some very helpful observations. This work was made possible by support received through ONR grant N00014-13-1-0174, program manager R. Joslin, and NSF grant CBET-1064257, managers H. Winter and D. Papavassiliou. B.G. acknowledges the support from the European Research Council under the European Union's Seventh Framework Programme (FP7/2007-2013), ERC grant agreement no. 277472.

REFERENCES

AFZAL, N. 1982 Fully developed turbulent flow in a pipe: an intermediate layer. *Ing.-Arch.* **52**, 355–377.

AFZAL, N. 1984 Mesolayer theory for turbulent flows. *AIAA J.* **22**, 437–439.

DEL ÁLAMO, J. C., JIMÉNEZ, J., ZANDONADE, P. & MOSER, R. D. 2004 Scaling of the energy spectra of turbulent channels. *J. Fluid Mech.* **500**, 135–144.

BAILEY, S. C., HULTMARK, M., SCHUMACHER, J., YAKHOT, V. & SMITS, A. J. 2009 Measurements of the dissipation scales in turbulent pipe flow. *Phys. Rev. Lett.* **103**, 014502.

BAILEY, S. C. C., KUNKEL, G. J., HULTMARK, M., VALLIKIVI, M., HILL, J. P., MEYER, K. A., TSAY, C., ARNOLD, C. B. & SMITS, A. J. 2010 Turbulence measurements using a nanoscale thermal anemometry probe. *J. Fluid Mech.* **663**, 160–179.

BAILEY, S. C. C. & SMITS, A. J. 2010 Experimental investigation of the structure of large- and very large-scale motions in turbulent pipe flow. *J. Fluid Mech.* **651**, 339–356.

BALAKUMAR, B. J. & ADRIAN, R. J. 2007 Large- and very-large-scale motions in channel and boundary-layer flows. *Phil. Trans. R. Soc. Lond.* A **365**, 665–681.

BANERJEE, T. & KATUL, G. G. 2013 Logarithmic scaling in the longitudinal velocity variance explained by a spectral budget. *Phys. Fluids* **25** (12), 125106.

CALAF, M., HULTMARK, M., OLDROYD, H. J., SIMEONOV, V. & PARLANGE, M. B. 2013 Coherent structures and the k^{-1} spectral behaviour. *Phys. Fluids* **25** (12), 125107.

CHIN, C., PHILIP, J., KLEWICKI, J., OOI, A. & MARUSIC, I. 2014 Reynolds-number-dependent turbulent inertia and onset of log region in pipe flows. *J. Fluid Mech.* **757**, 747–769.

CHUNG, D., MARUSIC, I., MONTY, J. P., VALLIKIVI, M. & SMITS, A. J. 2015 On the universality of inertial energy in the log layer of turbulent boundary layer and pipe flows. *Exp. Fluids* (submitted).

FIFE, P., KLEWICKI, J., MCMURTRY, P. & WEI, T. 2005 Multiscaling in the presence of indeterminacy: wall-induced turbulence. *Multiscale Model. Simul.* **4** (3), 936–959.

FIFE, P., KLEWICKI, J. & WEI, T. 2009 Time averaging in turbulence settings may reveal an infinite hierarchy of length scales. *J. Discrete Continuous Dyn. Syst.* A **24** (3), 781–807.

GAMARD, S. & GEORGE, W. K. 2000 Reynolds number dependence of energy spectra in the overlap region of isotropic turbulence. *Flow Turbul. Combust.* **63**, 443–477.

GANAPATHISUBRAMANI, B., LONGMIRE, E. K. & MARUSIC, I. 2003 Characteristics of vortex packets in turbulent boundary layers. *J. Fluid Mech.* **478**, 35–46.

GEORGE, W. K. & CASTILLO, L. 1997 Zero-pressure-gradient turbulent boundary layer. *Appl. Mech. Rev.* **50**, 689–729.

GEORGE, W. K. & TUTKUN, M. 2009 The mesolayer and Reynolds number dependencies of boundary layer turbulence. In *Progress in Wall Turbulence: Understanding and Modeling*, pp. 183–190. Springer.

GUALA, M., HOMMEMA, S. E. & ADRIAN, R. J. 2006 Large-scale and very-large-scale motions in turbulent pipe flow. *J. Fluid Mech.* **554**, 521–542.

GUALA, M., METZGER, M. & MCKEON, B. J. 2011 Interactions within the turbulent boundary layer at high Reynolds number. *J. Fluid Mech.* **666**, 573–604.

HÖGSTRÖM, U., HUNT, J. C. R. & SMEDMAN, A.-S. 2002 Theory and measurements for turbulence spectra and variances in the atmospheric neutral surface layer. *Boundary-Layer Meteorol.* **103** (1), 101–124.

HULTMARK, M. 2012 A theory for the streamwise turbulent fluctuations in high Reynolds number pipe flow. *J. Fluid Mech.* **707**, 575–584.

HULTMARK, M., VALLIKIVI, M., BAILEY, S. C. C. & SMITS, A. J. 2012 Turbulent pipe flow at extreme Reynolds numbers. *Phys. Rev. Lett.* **108** (9), 1–5.

HULTMARK, M., VALLIKIVI, M., BAILEY, S. C. C. & SMITS, A. J. 2013 Logarithmic scaling of turbulence in smooth- and rough-wall pipe flow. *J. Fluid Mech.* **728**, 376–395.

HUTCHINS, N. & MARUSIC, I. 2007 Evidence of very long meandering streamwise structures in the logarithmic region of turbulent boundary layers. *J. Fluid Mech.* **579**, 1–28.

JIMÉNEZ, J. M., HULTMARK, M. & SMITS, A. J. 2010 The intermediate wake of a body of revolution at high Reynolds numbers. *J. Fluid Mech.* **659**, 516–539.

KATUL, G. & CHU, C. R. 1998 A theoretical and experimental investigation of energy-containing scales in the dynamic sublayer of boundary-layer flows. *Boundary-Layer Meteorol.* **86** (2), 279–312.

KIM, K. C. & ADRIAN, R. J. 1999 Very large-scale motion in the outer layer. *Phys. Fluids* **11** (2), 417–422.

KLEWICKI, J. C. 2013*a* A description of turbulent wall-flow vorticity consistent with mean dynamics. *J. Fluid Mech.* **737**, 176–204.

KLEWICKI, J. C. 2013*b* Self-similar mean dynamics in turbulent wall-flows. *J. Fluid Mech.* **718**, 596–621.

KLEWICKI, J. C., FIFE, P. & WEI, T. 2009 On the logarithmic mean profile. *J. Fluid Mech.* **638**, 73–93.

KOLMOGOROV, A. N. 1941 The local structure of turbulence in incompressible viscous fluid for very large Reynolds numbers. *Dokl. Akad. Nauk SSSR* **30**, 301–305; reprinted in 1991. *Proc. R. Soc. Lond.* A **434**, 9–13.

KOVASZNAY, L. G., KIBENS, V. & BLACKWELDER, R. F. 1970 Large-scale motion in the intermittent region of a turbulent boundary layer. *J. Fluid Mech.* **41** (2), 283–325.

LONG, R. R. & CHEN, T.-C. 1981 Experimental evidence for the existence of the mesolayer in turbulent systems. *J. Fluid Mech.* **105**, 9–59.

MARUSIC, I. & KUNKEL, G. J. 2003 Streamwise turbulence intensity formulation for flat-plate boundary layers. *Phys. Fluids* **15**, 2461–2464.

MARUSIC, I., MCKEON, B. J., MONKEWITZ, P. A., NAGIB, H. M., SMITS, A. J. & SREENIVASAN, K. R. 2010 Wall-bounded turbulent flows: recent advances and key issues. *Phys. Fluids* **22**, 065103.

MARUSIC, I., MONTY, J. P., HULTMARK, M. & SMITS, A. J. 2013 On the logarithmic region in wall turbulence. *J. Fluid Mech.* **716**, R3.

MARUSIC, I., UDDIN, M. & PERRY, A. E. 1997 Similarity law for the streamwise turbulence intensity in zero-pressure-gradient turbulent boundary layers. *Phys. Fluids* **12**, 3718–3726.

MATHIS, R., HUTCHINS, N. & MARUSIC, I. 2009 Large-scale amplitude modulation of the small-scale structures in turbulent boundary layers. *J. Fluid Mech.* **628**, 311–337.

MCKEON, B. J. & MORRISON, J. F. 2007 Asymptotic scaling in turbulent pipe flow. *Phil. Trans. R. Soc. Lond.* A **365**, 771–787.

MONTY, J. P., HUTCHINS, N., NG, H. C. H., MARUSIC, I. & CHONG, M. S. 2009 A comparison of turbulent pipe, channel and boundary layer flows. *J. Fluid Mech.* **632**, 431–442.

MONTY, J. P., STEWART, J. A., WILLIAMS, R. C. & CHONG, M. S. 2007 Large-scale features in turbulent pipe and channel flows. *J. Fluid Mech.* **589**, 147–156.

MORRILL-WINTER, C. & KLEWICKI, J. 2013 Influences of boundary layer scale separation on the vorticity transport contribution to turbulent inertia. *Phys. Fluids* **25** (1), 015108.

MORRISON, J. F., MCKEON, B. J., JIANG, W. & SMITS, A. J. 2004 Scaling of the streamwise velocity component in turbulent pipe flow. *J. Fluid Mech.* **508**, 99–131.

MYDLARSKI, L. & WARHAFT, Z. 1996 On the onset of high-Reynolds-number grid-generated wind tunnel turbulence. *J. Fluid Mech.* **320**, 331–368.

NICKELS, T. B., MARUSIC, I., HAFEZ, S. M. & CHONG, M. S. 2005 Evidence of the k^{-1} law in a high-Reynolds-number turbulent boundary layer. *Phys. Rev. Lett.* **95**, 074501.

PERRY, A. E. & ABELL, C. J. 1977 Asymptotic similarity of turbulence structures in smooth- and rough-walled pipes. *J. Fluid Mech.* **79**, 785–799.

PERRY, A. E. & CHONG, M. S. 1982 On the mechanism of wall turbulence. *J. Fluid Mech.* **119**, 173–217.

PERRY, A. E., HENBEST, S. M. & CHONG, M. S. 1986 A theoretical and experimental study of wall turbulence. *J. Fluid Mech.* **165**, 163–199.

PERRY, A. E. & LI, J. D. 1990 Experimental support for the attached-eddy hypothesis in zero-pressure-gradient turbulent boundary layers. *J. Fluid Mech.* **218**, 405–438.

ROSENBERG, B. J., HULTMARK, M., VALLIKIVI, M., BAILEY, S. C. C. & SMITS, A. J. 2013 Turbulence spectra in smooth- and rough-wall pipe flow at extreme Reynolds numbers. *J. Fluid Mech.* **731**, 46–63.

SMITS, A. J. & MARUSIC, I. 2013 Wall-bounded turbulence. *Phys. Today* **66**, 25–30.

SMITS, A. J., MCKEON, B. J. & MARUSIC, I. 2011 High Reynolds number wall turbulence. *Annu. Rev. Fluid Mech.* **43**, 353–375.

SREENIVASAN, K. R. & SAHAY, A. 1997 The persistence of viscous effects in the overlap region and the mean velocity in turbulent pipe and channel flows. In *Self-Sustaining Mechanisms of Wall Turbulence* (ed. R. Panton), pp. 253–272. Comp. Mech. Publ.

TAYLOR, G. I. 1938 The spectrum of turbulence. *Proc. R. Soc. Lond.* A **164** (919), 476–490.

TOWNSEND, A. A. 1976 *The Structure of Turbulent Shear Flow*. Cambridge University Press.

VALLIKIVI, M. 2014 Wall-bounded turbulence at high Reynolds numbers. PhD Thesis, Princeton University.

VALLIKIVI, M., HULTMARK, M., BAILEY, S. C. C. & SMITS, A. J. 2011 Turbulence measurements in pipe flow using a nano-scale thermal anemometry probe. *Exp. Fluids* **51**, 1521–1527.

VALLIKIVI, M., HULTMARK, M. & SMITS, A. J. 2015 Turbulent boundary layer statistics at very high Reynolds number. *J. Fluid Mech.* (submitted).

VALLIKIVI, M. & SMITS, A. J. 2014 Fabrication and characterization of a novel nano-scale thermal anemometry probe. *Microelectromech. Syst. J.* **23** (4), 899–907.

VASSILICOS, J. C., LAVAL, J.-P., FOUCAUT, J.-M. & STANISLAS, M. 2014 The streamwise turbulence intensity in the intermediate layer of turbulent pipe flow. arXiv:1411.7276.

VINCENTI, P., KLEWICKI, J., MORRILL-WINTER, C., WHITE, C. M. & WOSNIK, M. 2013 Streamwise velocity statistics in turbulent boundary layers that spatially develop to high Reynolds number. *Exp. Fluids* **54**, 1629–1641.

WEI, T., FIFE, P., KLEWICKI, J. C. & MCMURTRY, P. 2005 Properties of the mean momentum balance in turbulent boundary layer, pipe and channel flows. *J. Fluid Mech.* **522**, 303–327.

WOSNIK, M., CASTILLO, L. & GEORGE, W. K. 2000 A theory for turbulent pipe and channel flows. *J. Fluid Mech.* **421**, 115–145.